HHS Public Access

Author manuscript

Chin J Chem. Author manuscript; available in PMC 2021 April 15.

Published in final edited form as:

Chin J Chem. 2019 November ; 37(11): 1167–1173. doi:10.1002/cjoc.201900177.

Order from Chaos: Self-Assembly of Nanoprism from a Mixture of Tetratopic Terpyridine-Porphyrin Conformers†

Alexander Filosa[a], **Heng Wang**[a], **Wei-Jian Li**[b], **Wenjing Zhang**[c], **Ellie Ngo**[a], **Jonathan E. Piccolo**[a], **Hai-Bo Yang**[b], **Xiaopeng Li**[*,a]

[a]Deportment of Chemistry, University of South Florida, 4202 Fowler Avenue, Tampa, Florida 33620, United States

[b]Shanghai Key Laboratory of Green Chemistry and Chemical Processes, School of Chemistry and Molecular Engineering, East China Normal University, 3663 N. Zhongshan Road, Shanghai 200062, China

[c]College of Chemistry and Molecular Engineering, Zhengzhou University, Zhengzhou, Henan 450001, China

Summary of main observation and conclusion

Porphyrins have been widely used in the self-assembly of metallo-supramolecules. In this study, we introduced 2,2':6,2"-terpyridine (tpy) into a porphyrin core to synthesize a tetratopic building block with multiple conformers. During the self-assembly with Zn(II), such a mixture of conformers was able to form a discrete nanoprism with all building blocks in one conformation. Detailed characterizations, including NMR, ESI-MS and traveling-wave ion mobility-mass spectrometry (TWIM-MS), all supported the formation of the desired assemblies. AFM and TEM further confirmed the dimensions of assembled nanoprisms. Moreover, the photophysical properties of the ligands and complexes were noticeably different depending upon size and metal ion center.

Background and Originality Content

Porphyrins are a vibrant class of organic dyes found widely in nature, ranging from the well-studied chlorophyll and heme found in the cells of plants and red blooded animals to the less known chlorocruoroporphyrin found in annelids.[1] Porphyrins in natural systems are as diverse in structure as they are in function. Heme[2] and chlorocruoroporphyrin[3] function as the core of oxygen transport proteins, which is responsible for transporting oxygen to vital systems; while chlorophyll provides necessary electron transport functions required for photosynthesis. As a result of millions of years of successive improvement, nature has perfected the function of porphyrins. In the field of synthetic chemistry, substitution and modification have been used to elicit specific functions of porphyrins. Free base porphyrins

†Dedicated to the special issue of "Supramolecular Chemistry".

* xiaopengli1@usf.edu.

Supporting Information

The supporting information for this article is available on the WWW under https://doi.org/10.1002/cjoc.201900177.

have been extensively studied in the biomedical fields, *e.g.*, clinical phototherapy and cancer imaging.[4] Metallo-porphyrins have been applied in sensors,[5] molecular electronics,[6] photovoltaic devices,[7] iono-phores[8] and catalysts.[9]

Much work has been done to increase the size, complexity and function of porphyrins with the goal of expanding the scope of porphyrin chemistry, using conventional covalent bonding and supramolecular self-assembly. For example, porphyrin tweezers[10] were constructed through the coordination with metal ions to control the capture and release of guest molecules. Supramolecular porphyrin boxes[11] and cages[12] with unique photodynamic properties could be applied to the fields of energy harvesting and cancer phototherapy. Porphyrin macrocycles[13] and prisms[14] were able to encapsulate large guest molecules and to achieve enrichment of specific fullerenes with high selectivity.[14b]

In coordination-driven self-assembly, most of the building blocks possess rigid geometry with single dominant conformation, which is able to prevent mismatching of the ligands, such as unwanted polymerization during the self-assembly.[15] It is rare to assemble discrete metallo-supramolecules using building blocks with multiple conformations. Herein, we report the construction of a porphyrin nanoprism through self-assembly of Zn(II) with 5,10,15,20-tetrakis(3-([2,2':6',2"-terpyridin]-4'-yl)phenyl)-7*H*,8*H*-porphyrin, which contains multiple conformational isomers. During the self-assembly, all the building blocks were converted into one conformation through coordination to achieve order from chaos. Detailed structural characterization confirmed that the conformations of building blocks were fixed within the metallo-supramolecular architecture. Further study showed that the photophysical properties of the ligands and complexes were noticeably different depending upon size and metal ion center.

Results and Discussion

Scheme 1a depicts the synthesis of a tetratopic tpy-porphyrin ligand (**L1**) through established methods.[16] Particularly, the porphyrin core was synthesized using the Adler-Longo method.[17] The metalated ligand (**L2**) was obtained by treating **L1** with 5 equivalents of zinc acetate in a 19 : 1 solution of chloroform and methanol followed by chelation with EDTA to remove the excess amount of Zn(II) attached to the tpy groups. It is worth noting that a longer version of tetratopic tpy-porphyrin was reported but with different synthetic strategy.[18] Our approach is a metal free synthesis, which avoids the multi-armed defects during Suzuki coupling and improves the separation.

NMR results of **L1** (Figure 1a, Figures S2–S5) provide evidence supporting the existence of isomers (Scheme 1b), which come from the steric repulsion of H^A-H^B and H^A-H^D during the rotation of tpy groups along phenyl-porphyrin C—C bond. Figure 2a displays a messy spectrum, especially in the region of δ 8.5–8.7, where the peaks are assigned to H^G and H^J on the tpy group. Such NMR shifts indicate the tpy groups in the tetratopic ligand are settled in various chemical environments, which are further supported by at least three distinct sets of H^I-H^J correlation signals in 2D-COSY spectra (Figure S5). Furthermore, we utilized traveling wave ion mobility-mass spectrometry (TWIM-MS)[19] to address the conformers in **L1**. Figure 2a shows the drift time distributions obtained from ion mobility separation of

ions at *m/z* 771, which corresponds to the $[\mathbf{L1}+2H^{+}]^{2+}$ species according to the isotope patterns (Figure 2b). Four distinct signal peaks at different drift times (*i.e.,* 2.70, 2.84, 3.05, and 3.32 ms, respectively) are observed in the spectrum, and correspond to four conformers of **L1** with different collision cross-section areas. Similarly, multiple sets of tpy proton resonance peaks (Figure 1c, Figures S6–S9) in ^{1}H NMR and multi-distributed signal bands in TWIM-MS (Figure S1) were also observed in **L2**, indicating that **L2** is also a mixture of conformers. The energy barrier for the rotation of one arm was studied by conformational search (Figure S31, detailed method was summarized in SI), which was calculated as 72.44 kJ-mol^{-1}. It is higher than the rotational energy of C—C in freely rotating *n*-butane (19 kJ-mol^{-1})[20] but lower than that of conformationally stabilized 1,1'-bi-2-naphthol (167 kJ-mol^{-1}).[21] Compared to the reported longer version of tetratopic tpy-porphyrin ligand, our design introduced more restriction to the rotation of tpy with a short arm, and constructed more compact structures with higher stability.[18]

Because of the dynamic nature of those four conformers, it is almost impossible to separate the conformers using regular column chromatography. Among the four possible conformers (L1-A to **L1-D**, Scheme 1b), **L1-A** could be the only candidate for constructing a discrete structure *via* coordination-driven self-assembly because of its introverted conformation. As a result, if we directly assemble the mixture of ligands with the stoichiometric amount of Zn(II), three circumstances could occur: (i) formation of polymeric assemblies; (ii) coexistence of discrete supramolecular architecture together with polymers; and (iii) generation of a pure discrete structure *via* conformational transformation from **L1-B/C/D** to **L1-A** during the assembly process.

After performing the assembly in $CHCl_3$/MeOH (*V/V* = 1/3) at 50 °C for 5 h, the product was precipitated by adding excessive NH_4PF_6 in MeOH solution, followed by several washings with water. Then the assemblies of **S1** and **S2** were obtained in high yields from **L1** and **L2**, respectively (Figures 3a and 3b), for further characterization. ESI-MS spectrum of **S1** (Figure 4a) displays one dominant set of peaks with continuous charge states from 6+ to 10+. The deconvoluted molecular mass of the assembly is 6749.8 Da, which agrees well with the molecular composition of three ligands, six zinc ions, and 12 PF_6^{-} as counterions, *viz.,* $[(C_{104}H_{66}N_{16})_3Zn_6\text{-}(PF_6)_{12}]$. The experimental isotope patterns are consistent with the theoretical ones based upon the chemical composition of **S1** (Figure 4a inset, Figure S24). We therefore proposed a supramolecular nanoprism with the simulated structure shown in Figures 3c and 3d. The possi- bility of forming the Zn-porphyrin (Zn-Por) complexes during the self-assembly of **S1** can be excluded by carefully controlling the amount of Zn(II). The undesired complexation does not occur because of the preference of forming the Zn-tpy complex rather than Zn-Por complex, even under the heating process, which was confirmed during our synthesis of **L2**.

ESI-MS of **S2** (Figure 4b) gave similar results and the corresponding isotope patterns are shown in Figure 4b inset and Figure S25, suggesting that a similar nanoprism was assembled (Figures 3e and 3f). In addition, a single band of signal at each charge state with narrow distribution is displayed in the TWIM-MS spectra of **S1** (Figure 4b) and **S2** (Figure 4d), which excludes the existence of isomers after the self-assembly. These results indicate that

all other conformers of **L1/L2** were converted to the introverted structure during the self-assembly process to form a discrete nanoprism structure (**S1/S2**).

Then multi-dimensional NMR spectroscopy was utilized to further identify the structure and purity of **S1** and **S2** (Figure 1, Figures S10–S23). After the self-assembly, the sharp and well-split peaks of supramolecules **S1** and **S2** instead of broad signals of **L1** and **L2** suggest that a discrete structure rather than polymeric assemblies is obtained. 2D-DOSY spectra of **S1** and **S2** (Figures 1e and 1f) display single narrowly distributed signal bands with diffusion coefficients (*D*) around 1.2×10^{-9} $m^2 \cdot s^{-1}$ (**S1**) and 1.0×10^{-9} m^2 s^{-1} (**S2**), respectively, further confirming the isomeric purity of the assemblies. More detailed analysis of the ^{1}H NMR spectra of **L2** and **S2**, for instance, shows characteristic downfield shift of H^f (δ ~0.05) and obvious upfield shift of H^j (δ ~1.0) after coordination, due to the electron deficiency of H^f and the electron shielding effect of H^j by the zinc ions,[22] respectively. In addition, the shifts of the protons on the phenyl spacer after coordination were observed.

The downfield shifts of $H^{a,c,e}$ (δ 0.2–0.4) were caused by the electron withdrawing effect from the coordination sites, while the abnormal electron shielding on H^d (δ ~0.1 towards upfield) is probably because the protons are located in the lateral faces of the nanoprism (Figure 3e). Notably, after coordination, the resonance signal of H^a was split into two sets after self-assembling into **S2**, indicating that H^a settled in two different environments, *i.e.,* the base surface (H^{a1}) and lateral surface (H^{a2}) of the prism. The same characteristic shifts and the splitting of H^A after assembly are also observed in the spectrum of **S1**.

A controlled self-assembly of **L1**/Zn(II) at lower temperature (0 °C) was conducted. The ^{1}H NMR spectrum (Figure S32a) of the complexes assembled at lower temperature displays a great number of undesired peaks in addition to the peaks of **S1**, which proves the formation of polymeric assemblies. The mixture was self-corrected to form pure **S1** after 3 h of heating at 50 °C (Figure S32b), owing to the dynamic transition among the **L1-A** to **L1-D** at higher temperature.

After removing the tpy-coordinated Zn(II) ions in **S1** and **S2** by mixing the supramolecular solution with EDTA under room temperature, the ^{1}H NMR spectra of the recovered ligands after chromatographic purification show exactly the same spectra with those of **L1/L2** before the assemblies. This further indicates that the transition potentials among the conformers are relatively low and dynamic, and thus drive the conformers into adopting the introverted conformation for forming the thermodynamically controlled nano-prism structure during the assembly.

Atomic Force Microscopy (AFM) and Transmission Electron Microscopy (TEM) were used to image individual supramolecular nanoprism. Individual dots were observed in both TEM and AFM images of **S1** (Figure 5) with a uniform molecular size. In the AFM images (Figures 5a–5c), the supramolecules are uniformly distributed. Using the section analysis on AFM, the height of the supramolecule is *ca.* 1.9 nm which shows a good correlation with the energy minimized model (Figure 3c). The AFM and TEM images of **S2** show similar results, which are summarized in Figure S26.

Concentration-dependence of forming **S1** and **S2** was carefully studied. ^{1}H NMR spectra of **S1** in various concentrations (Figure S27) show obvious changes by gradually decreasing the concentration. For instance, the peaks at σ 7.70, 9.19 and 9.30 shown at high concentration (5 mg/mL) gradually shrunk by lowering the concentration. Only one dominant set of peaks is displayed in the diluted (0.62 mg/mL) sample. Such a concentration-dependent variation was also observed in ESI-MS spectra (Figure S29), which helps us further determine all assembled structures. At a higher concentration (2.5 mg/mL), besides the dominant set of peaks assigned to **S1**, another two minor sets of peaks are also clearly observed, which are ascribed to tetramer (M4, $\mathbf{L1}_4Zn_8$) and pentamer (M5, $\mathbf{L1}_5Zn_{10}$), respectively. These two sets of signals gradually shrink and disappear by diluting the sample solution. The experiment shows that **S1** is the major structure in diluted solution.

However, no significant change was observed in the concentration-dependent experiments of **S2**, which showed one dominant set of signals in ^{1}H NMR spectra (Figure S28) and in ESI-MS spectra (Figure S30) under all concentrations. The significant difference in concentration-dependent behavior of **S1** and **S2** might come from the different flexibility of Zn free porphyrin and Zn-Por backbones. After coordination with Zn, the porphyrin ring backbone becomes more rigid and restricts any adjustment required to form the larger membered prisms.

Absorption and emission spectra of the ligands and supra-molecules were collected in $CHCl_3/CH_3CN$ (V/V = 1/9) mixed solvent for all ligands and supramolecules (Figure 6). The absorption spectra show a strong absorption band at around 420 nm, corresponding to the Soret bands of the porphyrinyl group. The indicative four Q bands are displayed in the UV-Vis of **L1** and **S1**, respectively, around 500–700 nm.[23] In the case of **L2** and **S2**, when Zn(II) is inserted into the porphyrin ring, the UV-Vis spectra exhibit two peaks instead of four in the Q regions, due to the modification in the symmetry of the substituted porphyrin ring from D_{2h} of **L1/S1** to the D_{4h} of **L2/S2**.[23] Two emission bands at 650 nm and 720 nm for **L1/S1** and 600 nm and 650 nm for **L2/S2** are observed in the emission spectra (Figure 6c). Obvious weaker emission spectra are shown in **L2/S2** compared with those of **L1/S1**, due to the additional zinc atom in the center of the emissive porphyrinyl chromophore.

Conclusions

Two new porphyrin-based tetratopic tpy ligands, **L1** and **L2**, were synthesized and proved to have multiple conformers under ambient temperature. Discrete supramolecular nanoprisms, **S1** and **S2**, instead of a mixture of polymers, were obtained through coordination-driven self-assembly from the mixture of conformers. Due to the dynamic transformation among these conformers, nanoprisms were constructed as the energy favorable structures by fixing all the ligands in one conformation. Therefore, this study provides another example of “order-out-of-chaos” through self-assembly.

Experimental

L1: P3 (2.19 g, 6.5 mmol) and propionic acid (20 mL) were added into a round bottom flask. The mixture was heated under 60 °C, pyrrole (0.52 g, 7.8 mmol) was added to the

mixture, then the mixture was heated at 145 °C for 3.5 h and cooled to room temperature. A 4 : 1 mixture of acetone and aqueous ammonia solution was added, and the flask was kept in a freezer overnight. The resultant precipitate was collected and washed with cold methanol 3 times. After being dried, the solid was further purified by chromatography on SiO_2 column with $CHCl_3$ as the eluent. 135 mg purple solid was obtained with a yield of 6%. ^{1}H NMR (400 MHz, $CDCl_3$) δ: 9.00 (s, 16H, $H^{A,F}$), 8.85 (s, 4H, H^D), 8.69–8.54 (m, 8H, $H^{G,J}$), 8.39–8.31 (m, 8H, $H^{B,E}$), 7.95 (t, J = 7.9 Hz, 4H, H^C), 7.85 (t, J = 8.5 Hz, 8H, H^H), 7.3 (t, J = 7.2 Hz, 8H, H^I), −2.60 (s, 2H, H^K) ^{13}C NMR (100 MHz, CDCl3) δ: 159.16, 156.15, 156.08, 150.17, 149.06, 142.95, 137.01, 136.71, 135.10, 133.18, 127.33, 126.76, 123.69, 121.25, 119.77, 119.31. ESI-MS (*m/z*): Calculated for $[C_{104}H_{66}N_{16}+2H]^{2+}$: 770.2906; found 770.2773.

L2: L1 (61.7 mg, 0.040 mmol) and $Zn(OAc)_26H_2O$ (59.6 mg, 0.2 mmol) were dissolved in a mixture of 19 mL $CHCl_3$ and 1 mL methanol, and the resultant mixture was heated for 5 h at 60 °C. The solvent was evaporated, and the residue was dissolved in DMF (20 mL). EDTA (59.6 mg, 0.16 mmol) was added into the DMF solution, and the mixture was stirred at room temperature for 2 d. The mixture was suspended in water and extracted by using $CHCl_3$. The organic phases were combined and evaporated. The residue was further purified by washing with cold acetone. 22.5 mg purple solid was obtained with a yield of 35%. ^{1}H NMR (400 MHz, $CDCl_3$) δ: 9.05 (s, 8H, H^f), 8.95 (s, 8H, H^a), 8.85 (s, 4H, H^d), 8.69–8.52 (m, 8H, H^{gJ}), 8.40–8.30 (m, 8H, $H^{b,e}$), 7.95 (t, J = 7.9 Hz, 4H, H^c), 7.85 (t, J = 9.7 Hz, 8H, H^h), 7.3 (t, J = 7.2 Hz, 8H, H^i). ^{13}C NMR (125 MHz, CDCl3) δ: 156.15, 156.06, 156.01, 155.94, 150.32, 150.26, 149.01, 148.96, 143.79, 136.82, 136.77, 136.72, 136.68, 135.08, 132.98, 132.15, 127.17, 126.45, 123.76, 123.70, 123.64, 121.35, 121.30, 121.25, 120.53, 119.35, 119.30. ESI-MS (*m/z*): Calculated for $[C_{104}H_{64}N_{16}Zn+2H]^{2+}$: 801.7474; found: 801.7339.

S1: L1 (3.0 mg, 1.9 μmol) was dissolved in 4 mL MeOH/$CHCl_3$ (3/1, *V/V*) solvent, and $Zn(NO_3)_2$-$6H_2O$ (1.2 mg, 3.9 μmol) was added in the above solution. The mixture was heated at 50 °C for 5 h, then precipitated in 10 mL NH_4PF_6 (80 mg 0.49 mmol) solution in MeOH. The solid was collected by centrifugation, washed with fresh methanol and water. After drying, 4.0 mg purple solid was obtained with a yield of 93%. ^{1}H NMR (500 MHz, CD_3CN) δ: 9.18 (s, 4H, H^F), 9.11 (s, 4H, H^F), 9.00 (s, 8H, H^A), 8.87 (d, J = 7.7 Hz, 4H, H^E), 8.69 (s, 4H, H^D), 8.57 (d, J = 8.0 Hz, 4H, H^B), 8.46 (d, J = 8.0 Hz, 8H, H^6), 8.31 (t, J = 7.7 Hz, 4H, H^C), 7.62–7.51 (m, 16H, $H^{I,H}$), 6.78 (dd, J = 7.7, 5.3 Hz, 8H, H^I), −2.75 (s, 2H, H^K). ^{13}C NMR (126 MHz, CD_3CN) δ: 157.21, 149.90, 148.11, 147.93, 143.42, 141.08, 135.81, 128.81, 127.90, 127.43, 123.46, 122.85, 120.18. ESI-MS (*m/z*): 979.72 $[M\text{-}6PF_6^-]^{6+}$ (calcd *m/z*: 979.68), 818.87 $[M\text{-}7PF_6^-]^{7+}$ (calcd *m/z*: 818.87), 698.25 $[M\text{-}8PF_6^-]^{8+}$ (calcd *m/z*: 698.27), 604.55 $[M\text{-}9PF_6^-]^{9+}$ (calcd *m/z*: 604.5S), 529.59 $[M\text{-}10PF_6^-]^{10+}$ (calcd m/z: 529.62).

S2: L2 (3.1 mg, 1.9 μmol) was dissolved in 4 mL MeOH/$CHCl_3$ (3/1, *V/V)* solvent, and $Zn(NO_3)_2$ $6H_2O$ (1.1 mg, 3.8 μmol) was added in the above solution. The mixture was heated at 50 °C for 5 h, then precipitated in 10 mL NH_4PF_6 (80 mg 0.49 mmol) solution in MeOH. The solid was collected by centrifugation, washed with fresh methanol and water. After drying, 3.9 mg purple solid was obtained, with a yield of 89%. ^{1}H NMR (500 MHz,

CD_3CN) δ: 9.03 (s, 4H, H), 9.01 (s, 4H, H^f), 8.91 (s, 8H, H^a), 8.73 (d, J = 7.6 Hz, 4H, H^e), 8.55 (s, 4H, H^d), 8.44 (d, J = 7.9 Hz, 4H, H^b), 8.37 (d, J = 8.1 Hz, 8H, H^g), 8.17 (t, J = 7.7 Hz, 4H, H^c), 7.59–7.48 (m, 16H,$H^{j,h}$), 7.59–7.48 (m, 16H, $H^{j,h}$), 6.70 (dd, J = 7.9, 5.1 Hz, 8H, H^i). ^{13}C NMR (125 MHz, CD3CN) δ: 156.99, 150.47, 149.89, 149.52, 147.73, 147.60, 144.32, 140.71, 135.83, 135.41, 135.15, 132.50, 132.10, 128.09, 127.05, 123.08, 122.70, 122.50, 120.14. ESI-MS (*m/z*): 846.08 $[M\text{-}7PF_6^-]^{7+}$ (calcd *m/z*: 816.12), 722.18 $[M\text{-}8PF_6^-]^{8+}$ (calcd *m/z:* 722.23), 626.04 $[M\text{-}9PF_6^-]^{9+}$ (calcd *m/z*: 625.99), 548.63 $[M\text{-}10PF_6^-]^{10+}$ (calcd *m/z*: 548.59), 485.57 $[M\text{-}11PF_6^-]^{11+}$ (calcd *m/z*: 485.54).

Supplementary Material

Refer to Web version on PubMed Central for supplementary material.

Acknowledgement

We gratefully acknowledge the support from the National Science Foundation (CHE-1506722) and National Institutes of Health (R01GM128037).

References

[1]. Lemberg R. Porphyrins in Nature. Progress in the Chemistry of Organic Natural Products, Ed.: Zechmeister L., Springer Vienna, Vienna, 1954, pp. 299–349.

[2]. Hamza I; Dailey HA One Ring to Rule Them All: Trafficking of Heme and Heme Synthesis Intermediates in the Metazoans. BBA-Mol. Cell Res. 2012, 1823, 1617–1632.

[3]. Fox HM; Gardiner JS The Oxygen Affinity of Chlorocruorin. Proc. Royal Soc. Lond. B 1932, 111, 356–363.

[4]. (a)Yoshioka E; Chelakkot VS; Licursi M; Rutihinda SG; Som J; Derwish L; King JJ; Pongnopparat T; Mearow K; Larijani M; Dorward AM; Hirasawa K. Enhancement of Cancer-Specific Protoporphyrin IX Fluorescence by Targeting Oncogenic Ras/MEK Pathway. Theranostics 2018, 8, 2134–2146; [PubMed: 29721068] (b)Rajora MA; Lou JWH; Zheng G. Advancing Porphyrin's Biomedical Utility via Supramolecular Chemistry. Chem. Soc. Rev. 2017, 46, 6433–6469; [PubMed: 29048439] (c)Naik A; Rubbiani R; Gasser G; Spingler B. Visible-Light-Induced Annihilation of Tumor Cells with Platinum-Porphyrin Conjugates. Angew. Chem. Int. Ed. 2014, 53, 6938–6941.

[5]. (a)Guillén MG; Gämez F; Roales J; Lopes-Costa T; Pinto SMA; Calvete MJF; Pereira MM; Pedrosa JM Molecular-Based Selection of Porphyrins Towards the Sensing of Explosives in the Gas Phase. Sens. Actuator B-Chem. 2018, 260, 116–124;(b)Fagadar-Cosma E; Vlascici D; Birdeanu M; Fagadar-Cosma G. Novel Fluorescent pH Sensor Based on 5-(4-Carboxy-phenyl)-10,15,20-tris-(phenyl)-porphyrin. Arab. J. Chem. 2014;(c)Lvova L; Di Natale C; Paolesse R. Porphyrin-Based Chemical Sensors and Multisensor Arrays Operating in the Liquid Phase. Sens. Actuator B-Chem. 2013, 179, 21–31.

[6]. (a)Limburg B; Thomas JO; Holloway G; Sadeghi H; Sangtarash S; Hou CYI; Cremers J; Narita A; Müllen K; Lambert CJ; Briggs GAD; Mol JA; Anderson HL Anchor Groups for Graphene-Porphyrin Single-Molecule Transistors. Adv. Funct. Mater. 2018, 28, 1803629;(b)Aoki T; Sakai H; Ohkubo K; Sakanoue T; Takenobu T; Fukuzumi S; Hasobe T. Ultrafast Photoinduced Electron Transfer in Face-to-Face Charge-Transfer π-Complexes of Planar Porphyrins and Hexaazatriphenylene Derivatives. Chem. Sci. 2015, 6, 1498–1509; [PubMed: 29308129] (c)Cho TJ; Shreiner CD; Hwang S-H; Moorefield CN; Courneya B; Godínez LA; Manríquez J; Jeong K-U; Cheng SZD; Newkome GR 5,10,15,20-Tetrakis [4'-(Terpyridinyl)phenyl]-porphyrin and Its Ru(II) Complexes: Synthesis, Photovoltaic Properties, and Self-assembled Morphology. Chem. Commun. 2007, 4456–4458.

[7]. (a)Bedioui F; Devynck J; Bied-Charreton C. Immobilization of Metalloporphyrins in Electropolymerized Films: Design and Applications. Acc. Chem. Res. 1995, 28, 30–36;(b)Walter

MG; Rudine AB; Wamser CC Porphyrins and Phthalocyanines in Solar Photovoltaic Cells. J. Porphyr. Phthalocyanines 2010, 14, 759–792;(c)Hasobe T; Imahori H; Kamat PV; Ahn TK; Kim SK; Kim D; Fujimoto A; Hirakawa T; Fukuzumi S. Photovoltaic Cells Using Composite Nanoclusters of Porphyrins and Fullerenes with Gold Nanoparticles. J. Am. Chem. Soc. 2005, 127, 1216–1228. [PubMed: 15669861]

[8]. Górski Ł ; Malinowska E; Parzuchowski P; Zhang W; Meyerhoff ME Recognition of Anions Using Metalloporphyrin-Based Ion-Selective Membranes: State-of-the-Art. Electroanalysis 2003, 15, 1229–1235.

[9]. Meng W; Breiner B; Rissanen K; Thoburn JD; Clegg JK; Nitschke JR A Self-Assembled M_8L_6 Cubic Cage that Selectively Encapsulates Large Aromatic Guests. Angew. Chem. Int. Ed. 2011, 50, 3479–3483.

[10]. (a)Biaiek MJ; Sprutta N; Latos-Grazynski L. Coordination-Induced Molecular Tweezing: Ruthenium Clusters Docked at Azuliporphyrinogens. Inorg. Chem. 2016, 55, 12061–12073; (b)Sun D; Tham FS; Reed CA; Chaker L; Boyd PDW Supramolecular Fullerene-Porphyrin Chemistry. Fullerene Complexation by Metalated “Jaws Porphyrin” Hosts. J. Am. Chem. Soc. 2002, 124, 6604–6612; [PubMed: 12047181] (c)Sun D; Tham FS; Reed CA; Chaker L; Burgess M; Boyd PDW Porphyrin-Fullerene Host-Guest Chemistry. J. Am. Chem. Soc. 2000, 122, 10704–10705.

[11]. (a)Otsuki J. Supramolecular Approach Towards Light-Harvesting Materials Based on Porphyrins and Chlorophylls. J. Mater. Chem. A 2018, 6, 6710–6753;(b)Wiester MJ; Ulmann PA; Mirkin CA Enzyme Mimics Based Upon Supramolecular Coordination Chemistry. Angew. Chem. Int. Ed. 2011, 50, 114–137.

[12]. Hong S; Rohman MR; Jia J; Kim Y; Moon D; Kim Y; Ko YH; Lee E; Kim K. Porphyrin Boxes: Rationally Designed Porous Organic Cages. Angew. Chem. Int. Ed. 2015, 54, 13241–13244.

[13]. (a)Tashiro K; Aida T; Zheng J-Y; Kinbara K; Saigo K; Sakamoto S; Yamaguchi A. Cyclic Dimer of Metalloporphyrin Forms a Highly Stable Inclusion Complex with C60. J. Am. Chem. Soc. 1999, 121, 9477–9478;(b)Zheng J-Y; Tashiro K; Hirabayashi Y; Kinbara K; Saigo K; Aida T; Sakamoto S; Yamaguchi K. Cyclic Dimers of Met-alloporphyrins as Tunable Hosts for Fullerenes: A Remarkable Effect of Rhodium(III). Angew. Chem. Int. Ed. 2001, 40, 1857–1861; (c)Shoji Y; Tashiro K; Aida T. Selective Extraction of Higher Fullerenes Using Cyclic Dimers of Zinc Porphyrins. J. Am. Chem. Soc. 2004, 126, 6570–6571. [PubMed: 15161282]

[14]. (a)Song J; Aratani N; Shinokubo H; Osuka A. A Porphyrin Nano-barrel That Encapsulates C60. J. Am. Chem. Soc. 2010, 132, 16356–16357;(b)Schmittel M; He B; Mal P. Supramolecular Multicomponent Self-Assembly of Shape-Adaptive Nanoprisms: Wrapping up C60 with Three Porphyrin Units Org. Lett. 2008, 10, 2513–2516; [PubMed: 18503275] (c)Fujita N; Biradha K; Fujita M; Sakamoto S; Yamaguchi K. A Porphyrin Prism: Structural Switching Triggered by Guest Inclusion. Angew. Chem. Int. Ed. 2001, 40, 1718–1721.

[15]. (a)Seidel SR; Stang PJ High-Symmetry Coordination Cages via Self-Assembly. Acc. Chem. Res. 2002, 35, 972–983; [PubMed: 12437322] (b)Chakrabarty R; Mukherjee PS; Stang PJ Supramolecular Coordination: Self-Assembly of Finite Two- and Three-Dimensional Ensembles. Chem. Rev. 2011, 111, 6810–6918; [PubMed: 21863792] (c)Cook TR; Stang PJ Recent Developments in the Preparation and Chemistry of Metallacycles and Metallacages via Coordination. Chem. Rev. 2015, 115, 7001–7045. [PubMed: 25813093]

[16]. (a)Loim NM; Kelbyscheva ES Synthesis of Dendrimers with Terminal Formyl Groups. Russ. Chem. Bull. 2004, 53, 2080–2085;(b)Noor A; Moratti SC; Crowley JD Active-Template Synthesis of “Click” [2]Rotaxane Ligands: Self-Assembly of Mechanically Interlocked Metallo-Supramolecular Dimers, Macrocycles and Oligomers. Chem. Sci. 2014, 5, 4283–4290;(c)Dess DB; Martin JC Readily Accessible 12-I-5 Oxidant for the Conversion of Primary and Secondary Alcohols to Aldehydes and Ketones. J. Org. Chem. 1983, 4155–4156.

[17]. (a)Lindsey JS; Wagner RW Investigation of the Synthesis of Ortho-Substituted Tetraphenylporphyrins. J. Org. Chem. 1989, 54, 828–836;(b)Lindsey JS; Schreiman IC; Hsu HC; Kearney PC; Marguerettaz AM Rothemund and Adler-Longo Reactions Revisited: Synthesis of Tetraphenylporphyrins under Equilibrium Conditions. J. Org. Chem. 1987, 52, 827–836.

[18]. Xie T-Z; Guo K; Li JY; Zhang B; Zheng K; Moorefield CN; Saunders MJ; Endres KJ; Sallam S; Wesdemiotis C; Newkome GR Coordination-Driven, Self-Assembly of a Polycyclic, Terpyridine-Based Nanobelt. J. Inorg. Organomet. Polym. Mater. 2016, 26, 907–913.

[19]. (a)Thalassinos K; Grabenauer M; Slade SE; Hilton GR; Bowers MT; Scrivens JH Characterization of Phosphorylated Peptides Using Traveling Wave-Based and Drift Cell Ion Mobility Mass Spectrometry. Anal. Chem. 2009, 81, 248–254; [PubMed: 19117454] (b)Li X; Chan Y-T; Newkome GR; Wesdemiotis C. Gradient Tandem Mass Spectrometry Interfaced with Ion Mobility Separation for the Characterization of Supramolecular Architectures. Anal. Chem. 2011, 83, 1284–1290. [PubMed: 21261266]

[20]. McMurry JE Organic Chemistry, 8th ed., Cengage Learning, Belmont, CA, 2012.

[21]. Tan JSJ; Paton RS Frontier Molecular Orbital Effects Control the Hole-Catalyzed Racemization of Atropisomeric Biaryls. Chem. Sci. 10, 2285–2289.

[22]. (a)Lu X; Li X; Cao Y; Schultz A; Wang J-L; Moorefield CN; Wesdemiotis C; Cheng SZD; Newkome GR Self-Assembly of a Supramolecular, Three-Dimensional, Spoked, Bicycle-like Wheel. Angew. Chem. Int. Ed. 2013, 52, 7728–7731;(b)Wang JL; Li X; Lu X; Hsieh IF; Cao Y; Moorefield CN; Wesdemiotis C; Cheng SZD; Newkome GR Stoichiometric Self-Assembly of Shape-Persistent 2D Complexes: A Facile Route to a Symmetric Supramacromolecular Spoked Wheel. J. Am. Chem. Soc. 2011, 133, 11450–11453.

[23]. Giovannetti R. The Use of Spectrophotometry UV/Vis for the Study of Porphyrins. In Macro to Nano Spectroscopy, Ed.: Uddin J, InTech, 2012.

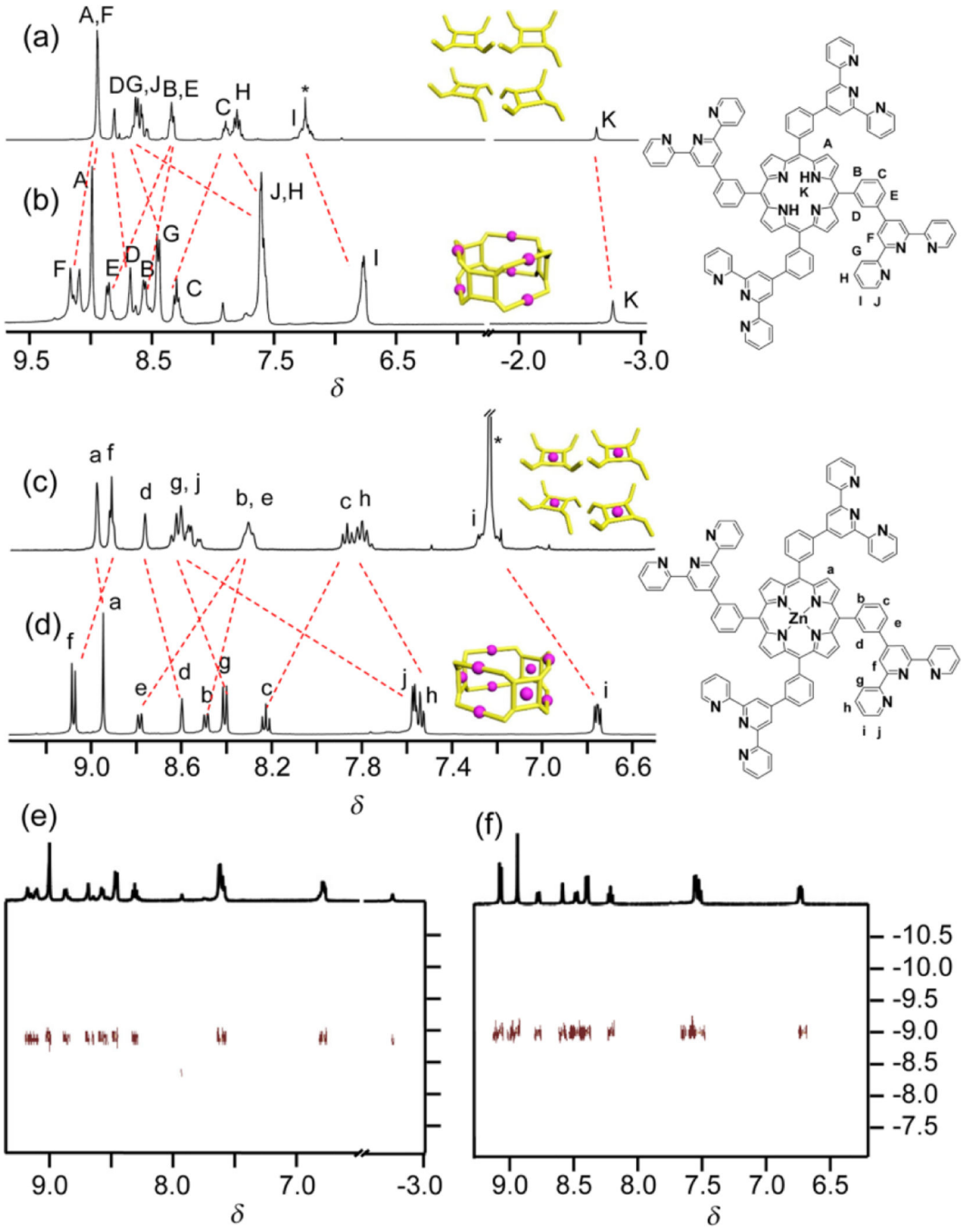

Figure 1.

^{1}H NMR spectra of (aromic region, 400 MHz, 300 K) (a) **L1** (in $CDCl_3$), (b) **S1** (*ca.* 1 mg/mL in CD_3CN), (c) **L2** (in $CDCl_3$), and (d) **S2** (*ca.* 1 mg/mL in CD_3CN) and 2D-DOSY spectra of (500 MHz, $CDCl_3$, 300 K) of (e) **S1** and (f) **S2** (aromic region). * Representing $CHCl_3$ in the solvent.

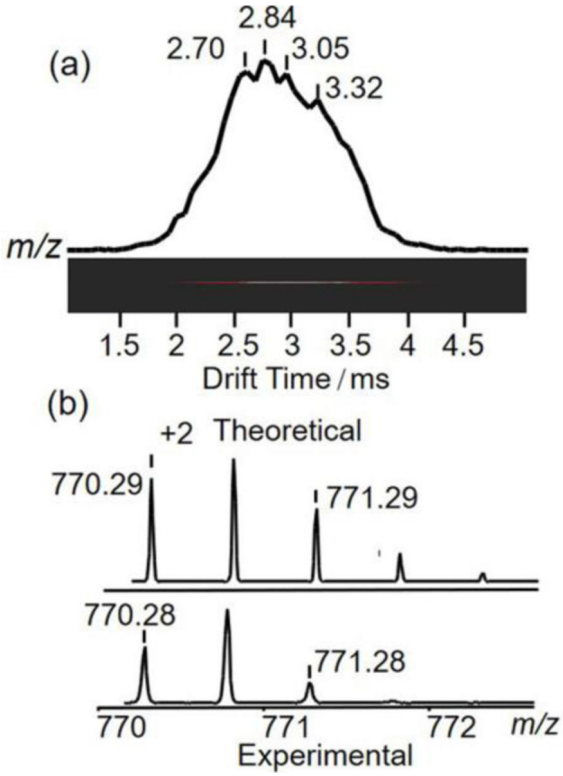

Figure 2.

(a) TWIM-MS spectrum of ions at *m/z* 771 for **L1**. Ion mobility separation gave signals at 2.70, 2.84, 3.05, and 3.32 ms, corresponding to four conformers of $[\mathbf{L1}+2H^{+}]^{2+}$, respectively. (b) Theoretical and experimental isotope patterns of the four separated peaks.

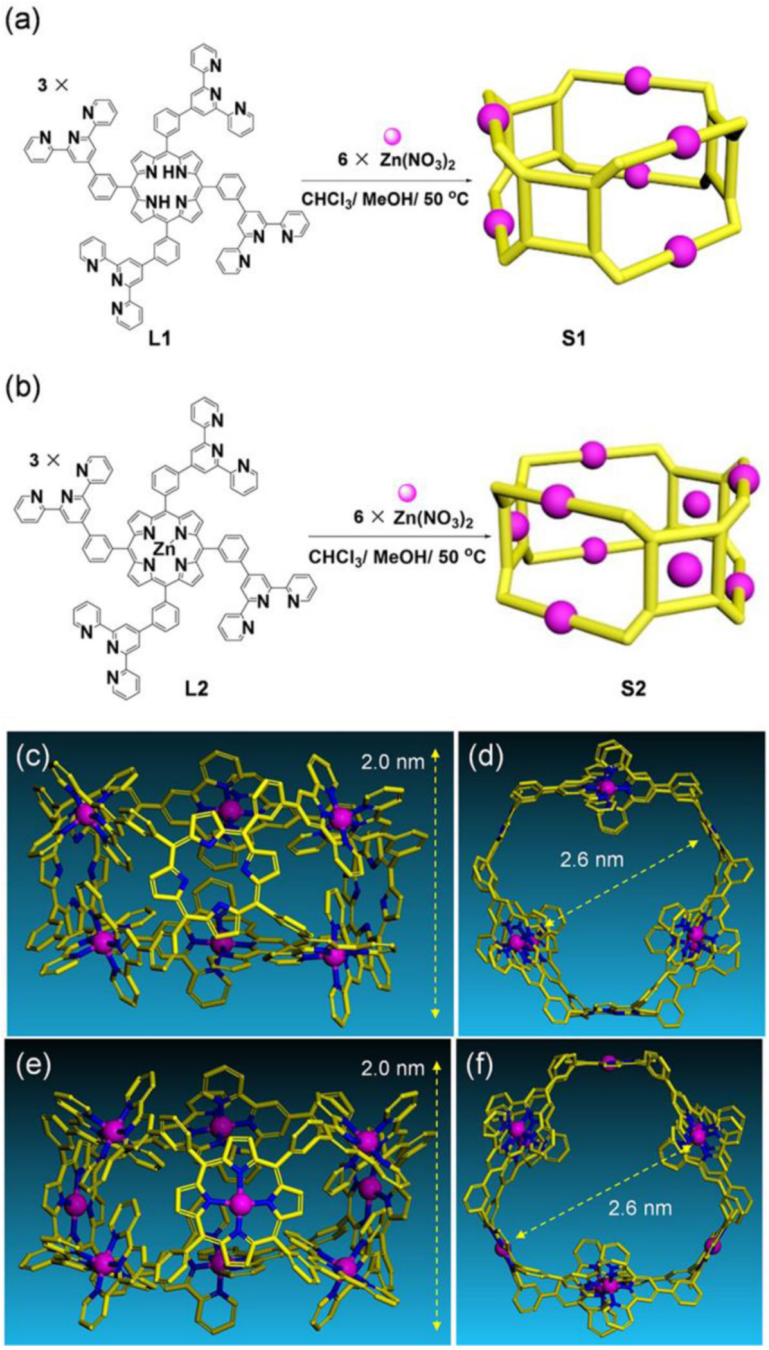

Figure 3.

Self-assembly of (a) supramolecular nanoprism **S1** and (b) **S2**; representative energy-minimized structures of **S1** (c, d) and **S2** (e, f) by molecular modeling.

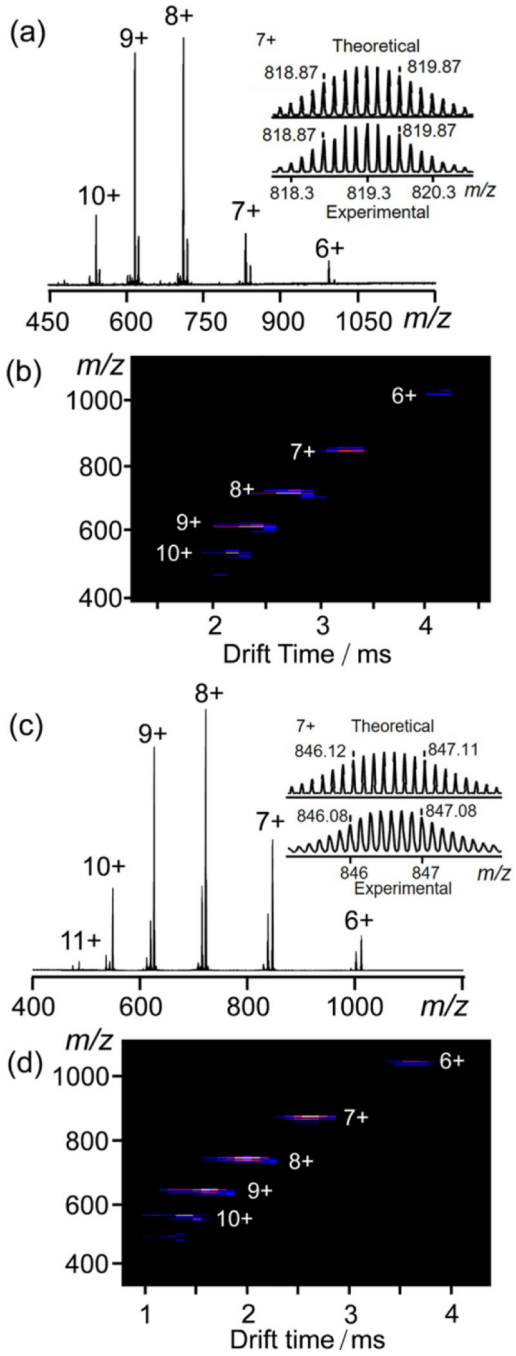

Figure 4.

ESI-MS of (a) **S1** and (c) **S2**. Insets are the theoretical and experimental isotope pattern of the species with 7+ charge state; TWIM-MS plots (*m/z* vs. drift time) of (b) **S1** and (d) **S2**.

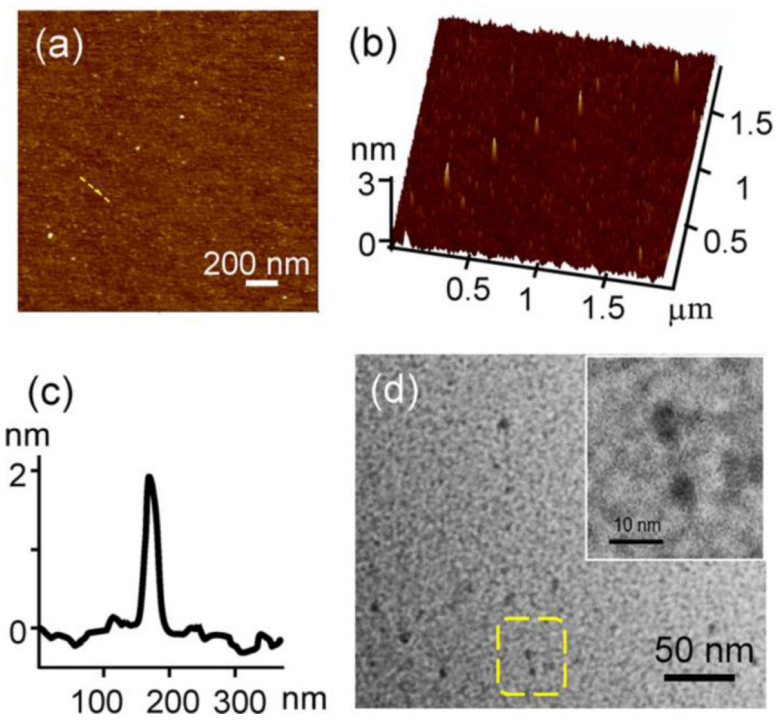

Figure 5.

(a) AFM image of **S1**, (b) 3D AFM image of **S1**, (c) Cross-section of one randomly selected particle in (a), (d) TEM images of **S1**, inset: zoomed-in TEM images of the selected area.

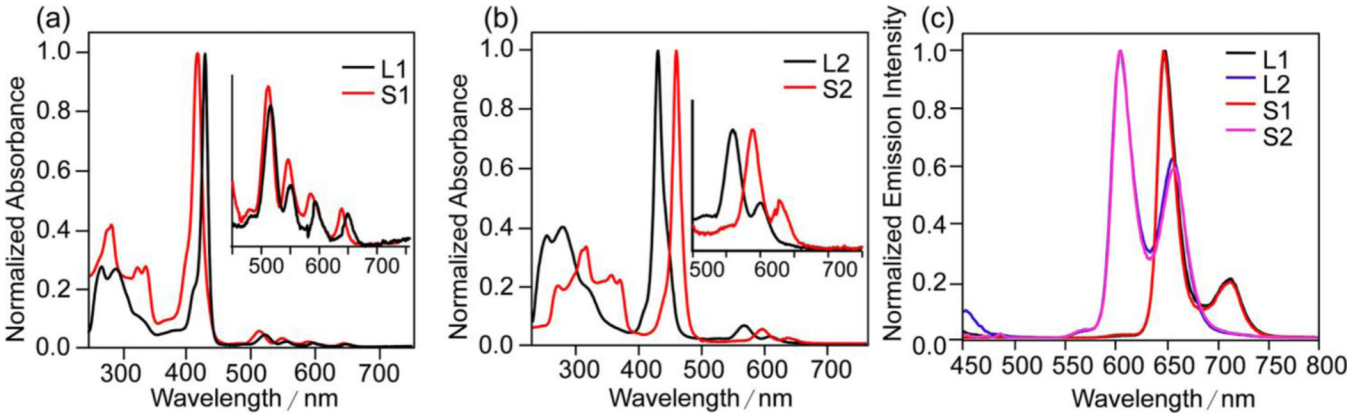

Figure 6.

UV-Vis absorption spectra for (a) **L1** and **S1**, (b) **L2** and **S2** (c = 10.0 μmol L^{-1}, solvent: 1 : 9 CHCI3/CH3CN); (c) émission spectra for **L1**, **L2**, **S1** and **S2** (λ_{ex} = 420 nm, c = 10.0 μmol L^{-1}, solvent: 1 : 9 $CHCI_3/CH_3CN$).

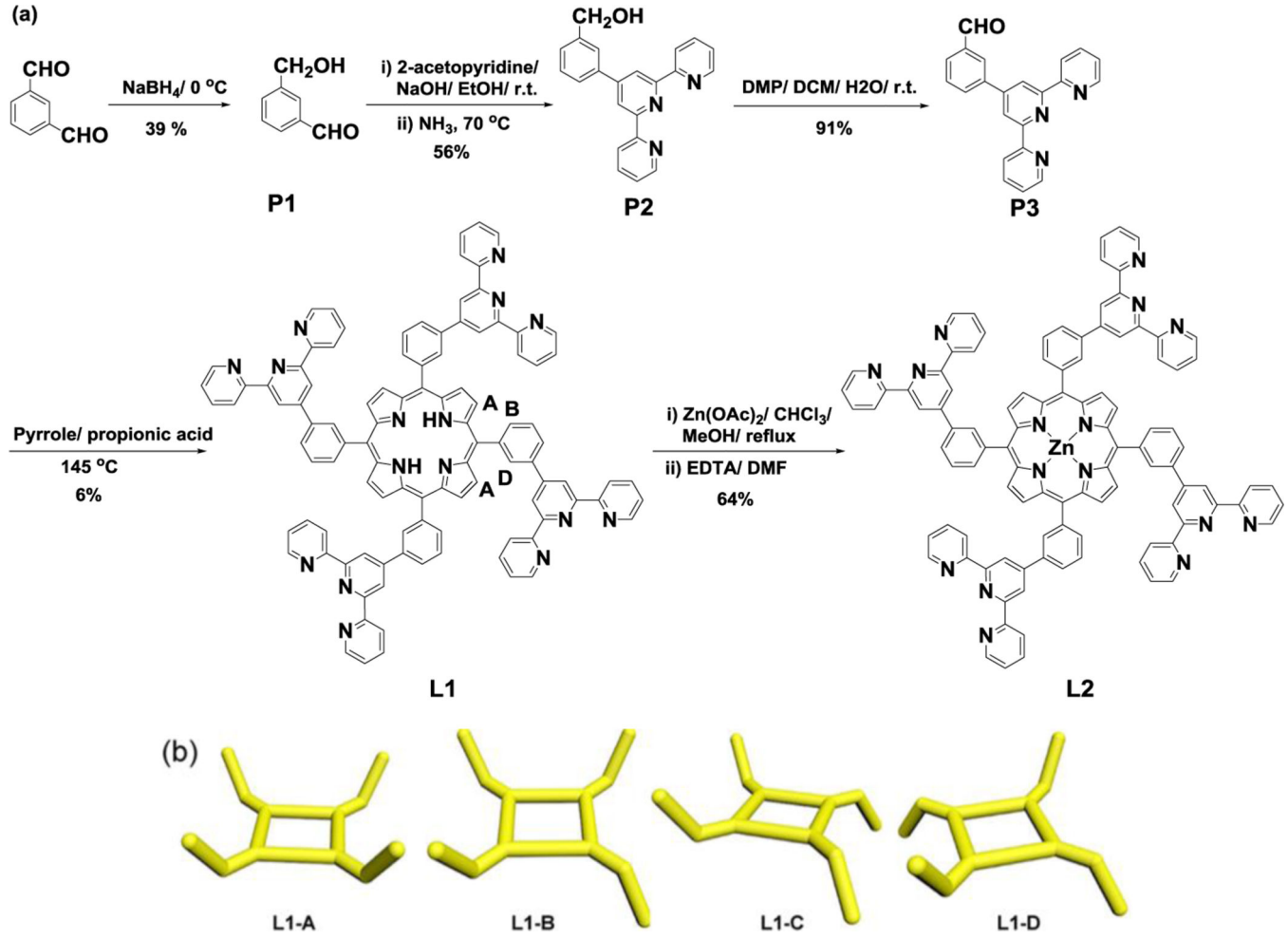

Scheme 1.

(a) Synthesis of tetratopic tpy-porphyrin ligands **L1** and **L2**. (B) Cartoons for the four conformers of **L1** (**L1-A** to **L1-D**) with different orientations of tpy